Biosensors and Bioelectronics 135 (2019) 82–87

Contents lists available at ScienceDirect

Biosensors and Bioelectronics

journal homepage: www.elsevier.com/locate/bios

Permselective glucose sensing with GLUT1-rich cancer cell membranes

Insu Kim, Dohyung Kwon, Dongtak Lee, Gyudo Lee**, Dae Sung Yoon*

School of Biomedical Engineering, Korea University, Seoul, 02841, Republic of Korea

ARTICLE INFO

Keywords:
Electrochemical analysis
Glucose biosensor
Cancer cell membrane
Glucose transporter-1
Permselectivity

ABSTRACT

Enzymatic blood glucose detection with selectivity is one of the most important conundrums, because human blood contains many components that can hinder enzyme-substrate reactions. Meanwhile, cancer cells express much higher levels of glucose transporter-1 on their cell membrane to selectively and excessively uptake more α-D-glucose than do normal cells. Inspired by such cellular permselectivity for glucose, herein we significantly improved the selectivity of a glucose sensor by using a breast cancer cell membrane (BCCM). The BCCM was extracted from MDA-MB-231 cells and coated onto an enzyme-deposited electrode *via* a vesicle fusion method. We investigated BCCM-coated sensors using ATR-FTIR, SEM, AFM, and cyclic voltammetry. The exceptional permselectivity of BCCM-coated sensors was validated using glucose solutions containing various interfering molecules (*e.g.*, D-(−)-fructose, D-(+)-xylose, D-(+)-maltose, L-cysteine, L-ascorbic acid, and uric acid) and human serum (4.35–7.35 mM of glucose), implying their high potential for practical use.

1. Introduction

Enzymatic electrochemical measurement of blood glucose has been widely employed because of its merits such as accuracy, sensitivity, linear response, and small volume of sample (Kim et al., 2007; Liu et al., 2012; Zhou et al., 2011). Despite these merits, achieving adequate selectivity is one of the biggest obstacles to glucose-selective measurement, because human blood contains a myriad of components, such as blood cells, proteins, saccharides, antioxidants, and ions (Cao et al., 2016; Farid et al., 2016; Huo et al., 2014; Shen et al., 2016; Yang et al., 2015). The selectivity of the conventional electrochemical glucose sensor is low mainly because enzymes (i.e., glucose oxidase and glucose dehydrogenase) cannot distinguish glucose from other similarly structured saccharides, such as fructose, xylose, and maltose. In addition, electrochemical detection is vulnerable to antioxidants, such as ascorbic acid, uric acid, and cysteine, that are abundant in blood (Raba and Mottola, 1995). These types of molecules (i.e., saccharides and antioxidants) are called interfering species that restrict accurate glucose sensing.

To filter or exclude these interfering species, there have been several attempts, including microdialysis of samples (e.g., serum and plasma) (Rogers et al., 2017; Su et al., 2017; Vargas et al., 2016) porous polymer-film deposition (Elizabeth et al., 2015; Gopalan et al., 2016; Lipani et al., 2018) and enzyme modification (Sode et al., 2017). Nevertheless, the low selectivity problem remains a challenge that needs to be improved for accurate blood glucose monitoring. Accordingly, improving the selectivity becomes a big concern with the advent of smart glucose sensors, such as wearable glucose sensors and continuous glucose monitoring systems.

Recently, it was reported that a red blood cell (RBC) membrane-coated glucose sensor allows glucose-specific permeability by expressing glucose transporter-1 (GLUT1) on the cell membrane (Kim et al., 2018). In principle, various kinds of phospholipids as main components of cell membranes can form lipid bilayers and hinder large and uncharged polar molecules (saccharides) and ions (antioxidants) from passing through the membrane (Deamer and Bramhall, 1986; Finkelstein, 1976), letting only α-D-glucose pass through the cell membrane *via* GLUT1 (Deng et al., 2014). This novel strategy can improve the selectivity and accuracy of glucose sensors compared to conventional electrochemical sensors. Despite these advantages, there are some fundamental limitations: i) RBCs cannot proliferate in vitro because they lack a nucleus and most organelles; ii) RBCs should be extracted from vertebrate; iii) characteristics of RBCs differ between donors; and iv) it is hard to keep biological consistency of RBCs, because of changes in the donor's physiological condition (Rosanwo et al., 2017). These drawbacks make it difficult to develop reliable RBC membrane-based biosensors without batch-to-batch variations.

To overcome these limitations, we employed a human breast cancer cell (MDA-MB-231). A great advantage of this cancer cell is that many fresh cells can be easily obtained. In addition, the characteristics of

* Corresponding author.
** Corresponding author.
E-mail addresses: lkd0807@korea.ac.kr (G. Lee), dsyoon@korea.ac.kr (D.S. Yoon).

https://doi.org/10.1016/j.bios.2019.04.007
Received 28 February 2019; Received in revised form 1 April 2019; Accepted 2 April 2019
Available online 12 April 2019
0956-5663/

these cells remain consistent. They are known to express a larger amount of GLUT1 than do normal cells (Soo et al., 2002; Venturelli et al., 2016). We speculate that if a GLUT1-rich breast cancer cell membrane (BCCM) is used as a permselective filter, it can improve the sensor's specificity and accuracy when measuring glucose in serum. In addition, the use of BCCM means that sensors can provide reliable signals, because they all employ BCCM originating from the same cell line. Herein, for the first time, we demonstrate that BCCM-coated glucose sensors can dramatically improve their permselectivity relative to uncoated ones. All sensors were tested with a glucose solution containing various interfering molecules (fructose, xylose, maltose, cysteine, ascorbic acid, and uric acid) (Balamurugan et al., 2017; Guo et al., 2017) and with human serum. Furthermore, we verified that our BCCM-coated glucose sensors exhibited excellent accuracy with long-term stability.

2. Experimental section

2.1. Reagents

Glucose, fructose, xylose, maltose, ascorbic acid, cysteine, uric acid, sodium phosphate monobasic, sodium phosphate dibasic, glucose hexokinase kit, and human serum were purchased from Sigma-Aldrich. Glucose sensors (ACCU-CHEK Performa, Roche) were purchased from Roche. Distilled water was purchased from Gibco. Phosphate buffer solution (0.1 M) was prepared by adding 0.1 M sodium phosphate dibasic into 0.1 M sodium monobasic until pH 7.4 was achieved. All solutions, such as a 2.5–15 mM glucose solution and fructose, xylose, maltose, ascorbic acid, cysteine, and uric acid solutions, were made with 0.1 M phosphate buffer solution. Ascorbic acid, uric acid, and cysteine were freshly made before measurement. Human serum was stored at −20 °C and thawed right before measurement. A high concentration of glucose was diluted in human serum to obtain a glucose concentration of 4.35–7.35 mM.

2.2. Apparatus

Morphologies of the uncoated sensor and BCCM-coated sensor were examined by scanning electron microscopy (SEM, JSM-6701F, JEOL) with high voltage (10 kV, 10 mA). Surface topologies of uncoated and BCCM-coated sensors were measured by atomic force microscopy (AFM, NX-10, Park systems). A PPP-NCHR probe was used for non-contact mode imaging. The scan rate was 0.5 Hz, and scan range was 30 μm. The surface roughness was calculated from four topology images using XEI software (Park Systems). A single layer of BCCM was prepared by the vesicle fusion method. Then 1% (v/v) BCCM solution diluted with distilled water was sonicated for 10 min in an ultrasonic bath to make BCCM vesicles. Then 200 μl of BCCM vesicle suspension was dropped onto freshly cleaved mica, which was incubated at 50 °C for 10 min. We made BCCM partially coated on mica to measure the height of the BCCM. To make BCCM fully coated, it was incubated for 30 min. The mica was washed with distilled water to remove floating BCCM vesicles. Cyclic voltammetry (CV) was performed using a potentiostat (Versastat3, AMETEK) controlled by VersaStudio software. All CVs were conducted at 25 mV/s scan rate and −0.1–0.4 V scan range. The scan rate was empirically chosen by measuring the CV (Fig. S1). Attenuated total refractive Fourier transform infrared spectroscopy (ATR-FTIR, spectrum 100, PerkinElmer) was used to analyze BCCM extracted from MDA-MB-231, the uncoated sensor, and the BCCM-coated sensor. Hydrodynamic diameters of BCCM vesicles were verified by dynamic light scattering (DLS, Zetasizer S90, Malvern). The thickness of the BCCM layer on a BCCM-coated sensor was measured by a stylus profiler (Alpha-step D100, KLA-Tencor).

2.3. Extraction of cell membrane from MDA-MB-231

MDA-MB-231 cell (breast cancer cells) was purchased from Korean Cell Line Bank (KCLB). MDA-MB-231 was cultured in a T75 culture flask with 5% CO_2 at 37 °C. We prepared cell culture media containing 90% MEM, 9% FBS, and 1% antibiotics (penicillin). The cell membrane was harvested with the following steps. A million of MDA-MB-231 cultured in the T75 flask were detached by trypsin-EDTA solution and transferred to a 50-ml conical tube. Cells were washed three times with pure 1X PBS followed by centrifugation. For hypotonic hemolysis, a cell pellet was suspended in ice-cold 0.25X PBS for 30 min. When hemolyzed, cell membrane fragments coexisted with various proteins and cellular components. To eliminate impurities, the hemolyzed suspension was washed three times with PBS by centrifugation at 20,000 *g* for 10 min. The white sediment of the breast cancer cell membrane was attained and frozen at −80 °C before use.

2.4. BCCM coating on sensors

The cell membrane was coated on glucose sensors using the previously reported method with a few modifications (Kim et al., 2018). Extracted BCCM membranes were diluted with distilled water to 1% (v/v) and sonicated for 10 min to make BCCM vesicles (like liposome or extracellular vesicles). The vesicle diameter was measured by dynamic light scattering. Then BCCM vesicle solutions were dropped onto the surface of the electrode and incubated at 50 °C for 30 min to induce vesicle fusion on the electrode.

3. Results and discussion

3.1. Schematic design of the BCCM sensor

Fig. 1 describes the permselective glucose-sensing mechanism of the BCCM-coated sensor. BCCM is thought to be mainly composed of two components: (1) phospholipid bilayers consisting of various phospholipids that act as a molecular diffusion barrier to prevent monosaccharides, disaccharides, and other molecules from passing through the membrane; and (2) various membrane proteins including a large amount of GLUT1 that make the membrane specifically permeable to glucose (Deng et al., 2014; Lee et al., 2018). Accordingly, we devised a BCCM-coated enzymatic glucose sensor on which reactions between the enzyme and glucose would not be affected by the many interfering molecules abundant in human blood, such as fructose, xylose, maltose, cysteine, uric acid, and ascorbic acid. We adopted pyrroloquinoline quinone-dependent glucose dehydrogenase (PQQ-GDH) as an enzyme. The detailed electrochemical reaction involved is shown below (Fender et al., 2012):

$$\text{D-Glucose} + \text{PQQ}_{ox}\text{-GDH} \rightarrow \text{D-Glucono-1,5-lactone} + \text{PQQ}_{re}\text{-GDH} \quad (1)$$

$$\text{PQQ}_{re}\text{-GDH} + \text{Mediator}_{ox} \rightarrow \text{PQQ}_{ox}\text{-GDH} + \text{Mediator}_{re} \quad (2)$$

where the subscripts *ox* and *re* represent the oxidized form and the reduced form, respectively.

We prepared and used BCCM following the previously reported method with a few modifications (Gao et al., 2013). Briefly, BCCM was extracted from MDA-MB-231 by hypotonic lysis and centrifugation. The BCCM was diluted with distilled water to 1% (v/v) and sonicated to form BCCM vesicles (Castellana and Cremer, 2006). A BCCM-derived vesicle was approximately 169 ± 11 nm in size (Fig. S1). These vesicles were then cast onto sensors by a vesicle fusion method (Mingeot-Leclercq et al., 2008).

3.2. Surface visualization of the BCCM-coated sensor

To investigate whether BCCM was properly coated onto sensors,

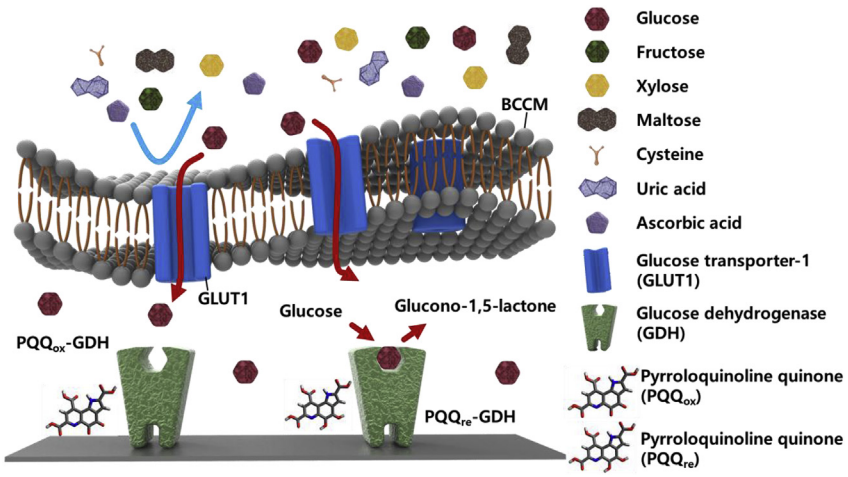

Fig. 1. Schematic illustration of the mechanism for the enzymatic glucose sensor coated with BCCM. The cell membrane acts as a molecular diffusion barrier that hinders large and uncharged molecules (fructose, xylose, and maltose) and ions (cysteine, uric acid, and ascorbic acid), whereas glucose is actively transported to enzymes via GLUT1. These enzymes then react with glucose without interference.

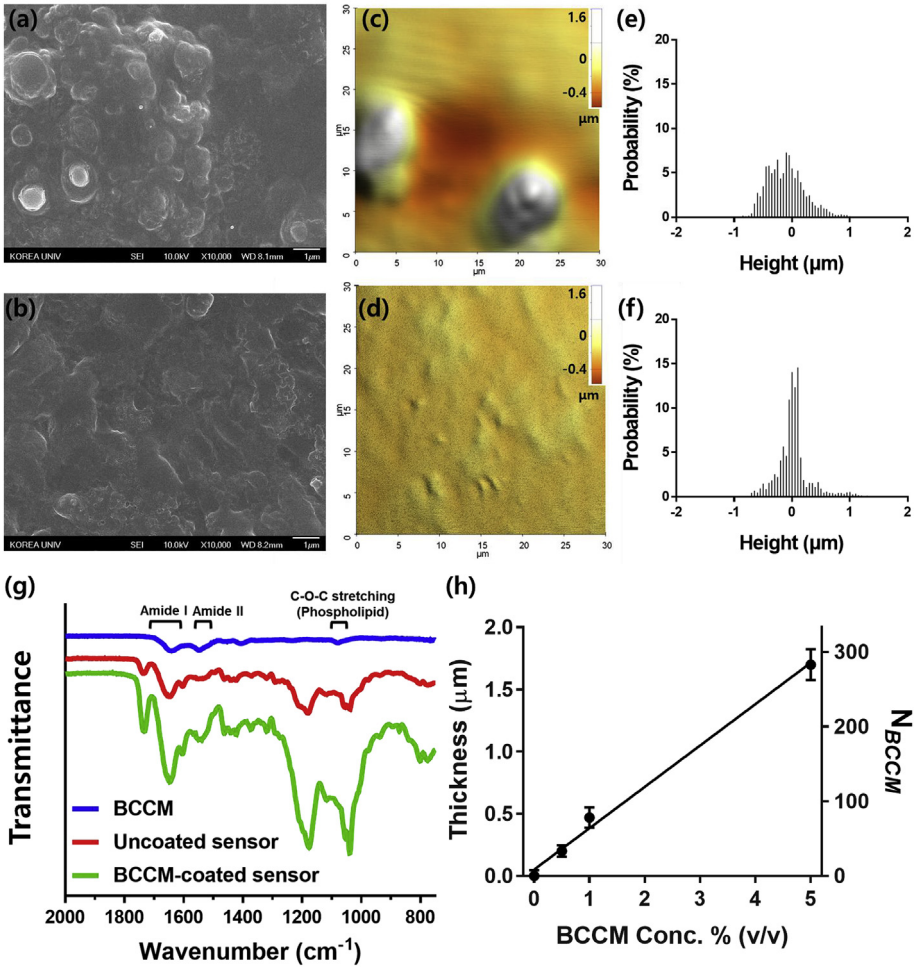

Fig. 2. SEM imaging of (a) uncoated sensor and (b) BCCM-coated sensor. AFM topographic images of (c) uncoated sensor and (d) BCCM-coated sensor (image size: $30 \times 30\,\mu m^2$). The height histogram of (e) uncoated sensor and (f) BCCM-coated sensor. (g) ATR-FTIR spectroscopy of BCCM solution (blue), uncoated sensor (green), and BCCM-coated sensor (red). (h) Thickness of each concentration of BCCM on the sensor and corresponding number of BCCM layers (N_{BCCM}). (For interpretation of the references to colour in this figure legend, the reader is referred to the Web version of this article.)

surfaces of both uncoated and BCCM-coated sensors were visualized using SEM and AFM (Fig. 2a–d). The surface of the uncoated sensor was composed of enzyme and non-reactive molecules (detailed composition of the enzyme complex is described in Fig. S2), resulting in a protruded and uneven surface. In contrast, the surface of a BCCM-coated sensor was smooth and even because of the depositing of BCCM layers. Its height distribution was analyzed using AFM images (Fig. 2e and f). Root-mean-squared roughness (R_q) of the sensor surface was 420 ± 100 nm for the uncoated sensor and 230 ± 30 nm for the BCCM-coated sensor. These R_q values indicate that the BCCM-coated sensor is almost twice as smooth as the uncoated sensor, implying that BCCM was evenly coated onto the sensor.

3.3. Characterization of the BCCM layer

We then conducted ATR-FTIR analysis to verify whether BCCM was well coated onto the sensor. Fig. 2g depicts ATR-FTIR spectra of the BCCM only, the uncoated, and the BCCM-coated glucose sensors. After coating, there were significant increments in the C-O-C stretching band (1,085–1,080 cm^{-1}), amide I (1,600–1,700 cm^{-1}), and amide II (1,510–1,580 cm^{-1}), indicating that the sensor was well covered with the BCCM including both phospholipids and membrane proteins (Derenne et al., 2014). It is confirmed that BCCM was well extracted from cells and coated onto the sensor (Gao et al., 2015; Tamm and Tatulian, 1997).

Next, we characterized the thickness of BCCM coating with different concentrations of BCCM suspension. It is known that the BCCM layer is thickened when BCCM concentration is increased in the deposition process (Kim et al., 2018). The thicknesses of BCCM coating for 0.5, 1, and 5% (v/v) BCCM solutions were 200 ± 47, 470 ± 81, and 1700 ± 120 nm, respectively (Fig. 2h). The thickness of a single BCCM layer was measured to be about 6 nm (Fig. S3) (Gao et al., 2013; Leonenko et al., 2000). This information is important in practice, because we can estimate the approximate number of BCCM layers (N_{BCCM}). To do so, the total thickness of BCCM was divided by that of a single layer. For 0.5, 1, and 5% (v/v) of BCCM solutions, N_{BCCM} layers were calculated to be 33 ± 8, 78 ± 13, and 290 ± 21, respectively.

3.4. Optimization of the thickness of the BCCM-coated sensor

To optimize the BCCM thickness of the sensors, we conducted a performance test, the result of which is shown in Fig. S4. For each BCCM-coated sensor with a different thickness, CV was conducted under various glucose concentrations ranging from 2.5 to 15 mM to cover normal to diabetic blood glucose levels. Measuring conditions for CV were a scan range from −0.1–0.4 V, and a scan rate of 25 mV/s (Fig. S5). Subsequently, we analyzed all data with linear regression to obtain the slope and limit of detection (LOD). The cathodic peak current (I_{pc}) was linearly proportional to the glucose concentration, regardless of the thickness of BCCM. From the result, both the slope and the LOD tended to be improved when the BCCM thickness increased up to approximately 470 nm (1% (v/v)). At 1,700 nm of BCCM, however, both the slope and the LOD drastically declined. This implies that there is an optimal thickness of BCCM coating for high glucose permeability. In our case, 470 nm of BCCM coating was thought to be the optimal one.

Fig. 3 depicts the performance test of the 470-nm BCCM-coated sensor, including CV and I_{pc}. The CV curve of the sensor shifted to positive as the glucose concentration increased. I_{pc} were 2.66 ± 0.04, 5.19 ± 0.02, 7.70 ± 0.09, 10.33 ± 0.02, and 15.54 ± 0.11 μA for 2.5, 5, 7.5, 10, and 15 mM of glucose, respectively. We also checked whether the cathodic peak potential at I_{pc} has some relation with the glucose concentration, the result of which is shown in Fig. S6. The linear regression analysis showed that all the data points best fit with a linear equation (R^2 = 0.9948), which indicates that the cathodic peak potential was proportional to the glucose concentration (Elgrishi et al., 2018). The LOD of a 470-nm BCCM-coated sensor was estimated to be ~0.24 mM, which was about 1.9 and 4 times better than those of an uncoated sensor (~0.46 mM) and an RBC membrane-coated sensor (~1.06 mM) (Kim et al., 2018), respectively. Further experiments for performance tests have all been done using the 470-nm BCCM-coated sensors.

3.5. Selectivity test of BCCM-coated sensor

We tested BCCM-coated sensors to evaluate their specificity in the presence of various interfering molecules, such as fructose, xylose, maltose, cysteine, ascorbic acid, and uric acid (Fig. S7). We prepared pure test solutions of each interfering reagent (5 mM fructose, 5 mM xylose, 1 mM maltose, 1 mM cysteine, 1 mM ascorbic acid, and 0.5 mM uric acid) (Raba and Mottola, 1995). We set the concentration of each interfering molecule higher than that in a normal human physiological condition to verify the selectivity of our sensors. After measuring the signal intensity of each test solution, we calculated its relative intensity to that of a pure 5 mM glucose solution. The relative intensity of uncoated sensors ranged from 5.63 to 29.42% depending on the type of interfering reagent. In contrast, BCCM-coated sensors exhibited much lower relative intensity (1.77–7.74%), indicating that BCCM effectively impeded the penetration of each interfering reagent. Likewise, we performed further practical selectivity tests for a competitive enzyme-substrate reaction using mixture solutions (5 mM glucose + each interfering reagent). In detail, each mixture solution was made to have 5 mM glucose plus 5 mM fructose, 5 mM xylose, 1 mM maltose, 1 mM cysteine, 1 mM ascorbic acid, or 0.5 mM uric acid. Results are shown in Fig. 4. Remarkably, the BCCM-coated sensors were very specific to glucose for all mixture solutions, displaying very low variations (0–4%) regardless of the existence of interfering molecules. However, uncoated sensors significantly responded to each interfering reagent. Relative intensities of uncoated sensors considerably differed, showing 6.2–35.8% variations depending on the type of interfering reagent. Taken together, these results confirmed that the use of BCCM for sensors could prevent the penetration of interfering reagents. In addition, their selectivity for glucose was dramatically improved over that of uncoated sensors.

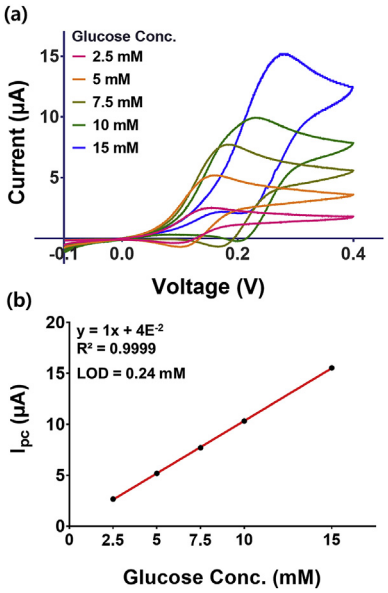

Fig. 3. (a) Cyclic voltammogram of BCCM-coated sensor in the presence of 2.5–15 mM glucose in 0.1 M phosphate buffer solution. (b) Cathodic peak current (I_{pc}) plots taken from (a). Data were fitted by linear regression equation. Error bars at each point are much shorter than the size of the symbol (●) and so are omitted. Each data point represents triplicate measurements.

3.6. Glucose detection in human serum

Last, glucose level in human serum was measured with our BCCM-coated sensors. Results are summarized in Table 1. The original glucose concentration of the serum was verified to be 4.35 mM by a commercial glucose hexokinase kit (Bondar and Mead, 1974). We then added extra glucose into the original serum. The final glucose concentrations were adjusted to 5.85 and 7.35 mM. We tested human serum containing 4.35, 5.85, and 7.35 mM glucose. Results were compared to the calibration curve of the BCCM-coated sensors made by using pure glucose solutions (4.35, 5.85, and 7.35 mM). The glucose concentration of each human serum was estimated to be 4.37 ± 0.06, 5.81 ± 0.07, and 7.45 ± 0.03 mM, respectively, with a percentage of error of

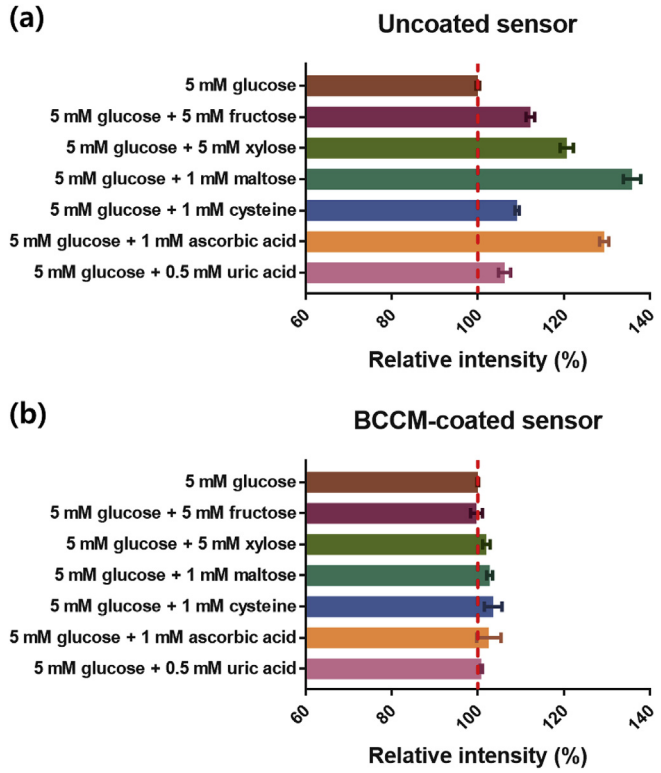

Fig. 4. Selectivity test of (a) uncoated sensor and (b) BCCM-coated sensor for mixture solutions of 5 mM of glucose and each interfering molecule. The intensity of 5 mM glucose is set to be 100% and the red dashed line represents 100%. Concentrations of each interfering molecule are as follows: 5 mM fructose, 5 mM xylose, 1 mM maltose, 1 mM cysteine, 1 mM ascorbic acid, and 0.5 mM uric acid. Each data point represents triplicate measurements. (For interpretation of the references to colour in this figure legend, the reader is referred to the Web version of this article.)

Table 1
Serum glucose measurement of BCCM-coated sensor. The original glucose concentration was 4.35 mM. Additional glucose was added to the serum to make 5.85 and 7.35 mM. The result from the BCCM-coated sensor was calculated as a percentage error.

#	Glucose conc. in serum (mM)	Measured glucose conc. (mM)	Percent error (%)
1	4.35	4.37 ± 0.06	0.46 ± 1.38
2	5.85	5.81 ± 0.07	0.07 ± 1.20
3	7.35	7.45 ± 0.03	1.36 ± 0.41

0.46 ± 1.38, 0.07 ± 1.20, and 1.36 ± 0.41%, respectively. All these cases exhibited very small errors (0.07–1.36%) between the measured glucose level and the actual level. This indicates that our BCCM-coated sensors have excellent reliability and selectivity even in a medium containing numerous types of interfering molecules such as human serum.

Because cell membrane can act as a diffusion barrier to prevent transport of other molecules and isolate the sensor electrode from the environment, we speculate that BCCM coating can help sensors to retain long-term stability without any deterioration caused by the environment. For example, the activity of the enzyme decreased when the enzymatic glucose sensors were exposed to moisture in the air (Chen et al., 2008; Valdes and Moussy, 2000). Accordingly, the enzymatic glucose sensors remain relatively unaffected by water, if the BCCM is coated onto the sensor. To verify whether this speculation is true, we tested the long-term stability of BCCM-coated sensors with different exposure time to ambient condition. To this end, we stored both the uncoated and the BCCM-coated sensors at 22 °C in an automatic desiccator cabinet and then tested both sensors with 2.5, 5.0, and 7.5 mM glucose solutions after four weeks (Fig. 5a and b). When tested after four weeks, the uncoated sensors exhibited a 6.79, 8.67, and 8.31% error in comparison with the fresh sensor, whereas the BCCM-coated sensors showed 2.52, 0.26, and 4.29% errors, respectively (Fig. 5c). This implies that BCCM coating can preserve sensor electrodes and make them display reliable performance over a long period of time. Moreover, the sensitivity was calculated from Fig. 5a and b. The sensitivity of uncoated sensors was reduced by 16% from that of the fresh sensor, whereas that of the BCCM-coated sensors was decreased by 6% (less deterioration in sensitivity). The linearity (R^2) of the plot was 0.9647 for the uncoated sensors and 0.9979 for the BCCM-coated sensors. Taken together, these results confirmed that the BCCM-coated sensors worked better than did the uncoated sensors in many aspects (*e.g.*, stability, sensitivity, and linearity after four weeks). These improvements resulted because BCCM prevents the enzyme denaturation caused by the environment and maintains the enzyme's activity.

4. Conclusion

In summary, we present a novel GLUT1-rich cell membrane-based glucose sensor that shows excellent permselectivity and reliability. In the experiment, 470-nm-thick BCCM (~78 layers) was found to be optimal for a permselective diffusion barrier, in which BCCM effectively impeded the penetration of interfering molecules without affecting the glucose permeability. Accordingly, the use of BCCM made our enzymatic glucose sensors highly permselective to glucose in the presence of various interfering reagents such as saccharides and antioxidants. In detail, the BCCM layers contributed to remarkable improvement of reliability; from 6.2 to 35.8% (uncoated) to 0–3.9% (coated) in percentage error. Furthermore, the BCCM-coated sensors were very reliable and accurate at glucose detection (0.07–1.36% in error) even in a medium containing numerous types of interfering molecules, like human serum. Although the cancer cell membrane is an effective biomaterial for improving the selectivity of the glucose sensor, there are several critical prerequisites for taking advantage of the membrane: i) The phenotypes of cells should be maintained to make sensing performance consistent (Kroll et al., 2017); ii) The cell membrane should be purified properly by eliminating cell organelles and cytosolic components (Hu et al., 2015); iii) The thickness of the BCCM layers should be

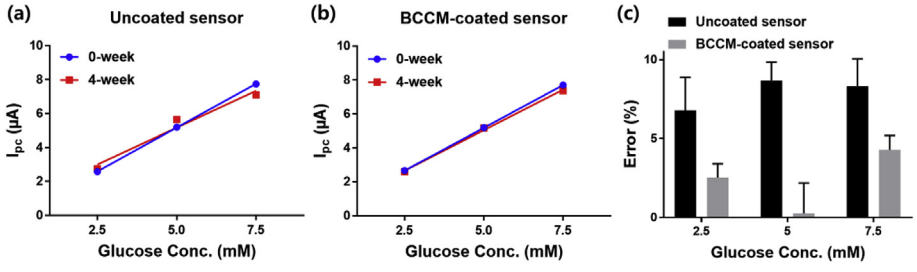

Fig. 5. Long-term stability test of (a) uncoated sensor and (b) BCCM-coated sensor. Blue dots and lines represent the I_{pc} at 0-week (i.e., freshly made sensors). Red square and lines represent I_{pc} for 4-week stored sensors. Each data point represents triplicate measurements. Error bars at each point are much shorter than the size of the symbol (● and ■) and so are omitted. Each data point represents triplicate measurements. The I_{pc} for each glucose concentration are summarized in Fig. S8. (c) Errors of 4-week-stored sensors from freshly made sensors. (For interpretation of the references to colour in this figure legend, the reader is referred to the Web version of this article.)

optimized for the type of sensors (Kim et al., 2018). Our results support that adopting BCCM as a glucose-permselective material may also be useful in practice to improve the selectivity of both invasive and non-invasive glucose sensors for continuous real-time monitoring.

CRediT authorship contribution statement

Insu Kim: Conceptualization, Methodology, Data curation, Writing - original draft. **Dohyung Kwon:** Validation, Formal analysis. **Dongtak Lee:** Formal analysis, Writing - original draft. **Gyudo Lee:** Supervision, Funding acquisition, Writing - review & editing. **Dae Sung Yoon:** Supervision, Project administration, Funding acquisition, Writing - review & editing.

Acknowledgments

This work was supported by the National Research Foundation of Korea Grant funded by the Korean Government (MSIP) (No. NRF-2016R1A2B4010269, NRF-2017R1A6A3A11034311 and NRF-2018M3C1B7020722). This material is also supported by the Ministry of Trade, Industry and Energy under Industrial Technology Innovation Program (No.10079316). Dr. Gyudo Lee is thankful for the financial support by the Korea University Grant.

Appendix A. Supplementary data

Supplementary data to this article can be found online at https://doi.org/10.1016/j.bios.2019.04.007.

References

Balamurugan, J., Thanh, T.D., Karthikeyan, G., Kim, N.H., Lee, J.H., 2017. A novel hierarchical 3D N-Co-CNT@NG nanocomposite electrode for non-enzymatic glucose and hydrogen peroxide sensing applications. Biosens. Bioelectron. 89, 970–977.
Bondar, R.J.L., Mead, D.C., 1974. Evaluation of glucose-6-phosphate dehydrogenase from < em > Leuconostoc mesenteroides < /em > in the hexokinase method for determining glucose in serum. Clin. Chem. 20 (5), 586.
Cao, X., Wang, K., Du, G., Asiri, A.M., Ma, Y., Lu, Q., Sun, X., 2016. One-step electrodeposition of a nickel cobalt sulfide nanosheet film as a highly sensitive nonenzymatic glucose sensor. J. Mater. Chem. B 4 (47), 7540–7544.
Castellana, E.T., Cremer, P.S., 2006. Solid supported lipid bilayers: from biophysical studies to sensor design. Surf. Sci. Rep. 61 (10), 429–444.
Chen, J., Zhang, W.-D., Ye, J.-S., 2008. Nonenzymatic electrochemical glucose sensor based on MnO2/MWNTs nanocomposite. Electrochem. Commun. 10 (9), 1268–1271.
Deamer, D.W., Bramhall, J., 1986. Permeability of lipid bilayers to water and ionic solutes. Chem. Phys. Lipids 40 (2), 167–188.
Deng, D., Xu, C., Sun, P., Wu, J., Yan, C., Hu, M., Yan, N., 2014. Crystal structure of the human glucose transporter GLUT1. Nature 510 (7503), 121–125.
Derenne, A., Vandersleyen, O., Goormaghtigh, E., 2014. Lipid quantification method using FTIR spectroscopy applied on cancer cell extracts. Biochim. Biophys. Acta Mol. Cell Biol. Lipids 1841 (8), 1200–1209.
Elgrishi, N., Rountree, K.J., McCarthy, B.D., Rountree, E.S., Eisenhart, T.T., Dempsey, J.L., 2018. A practical beginner's guide to cyclic voltammetry. J. Chem. Educ. 95 (2), 197–206.
Elizabeth, W.M., Thomas, D., Christophe, B., G, M.G., K, O.C., 2015. A glucose sensor via stable immobilization of the GOx enzyme on an organic transistor using a polymer brush. J. Polym. Sci. A Polym. Chem. 53 (2), 372–377.
Farid, M.M., Goudini, L., Piri, F., Zamani, A., Saadati, F., 2016. Molecular imprinting method for fabricating novel glucose sensor: polyvinyl acetate electrode reinforced by MnO2/CuO loaded on graphene oxide nanoparticles. Food Chem. 194, 61–67.
Fender, J.E., Bender, C.M., Stella, N.A., Lahr, R.M., Kalivoda, E.J., Shanks, R.M.Q., 2012. Serratia marcescens quinoprotein glucose dehydrogenase activity mediates medium acidification and inhibition of prodigiosin production by glucose. Appl. Environ. Microbiol. 78 (17), 6225–6235.
Finkelstein, A., 1976. Water and nonelectrolyte permeability of lipid bilayer membranes. J. Gen. Physiol. 68 (2), 127–135.
Gao, W., Hu, C.-M.J., Fang, R.H., Luk, B.T., Su, J., Zhang, L., 2013. Surface functionalization of gold nanoparticles with red blood cell membranes. Adv. Mater. 25 (26), 3549–3553.
Gao, Y., Huo, X., Dong, L.I.U., Sun, X., Sai, H.E., Wei, G., Xu, Y., Zhang, Y., Wu, J., 2015. Fourier transform infrared microspectroscopy monitoring of 5-fluorouracil-induced apoptosis in SW620 colon cancer cells. Mol. Med. Rep. 11 (4), 2585–2591.
Gopalan, A.I., Muthuchamy, N., Komathi, S., Lee, K.P., 2016. A novel multicomponent redox polymer nanobead based high performance non-enzymatic glucose sensor. Biosens. Bioelectron. 84, 53–63.
Guo, Q., Liu, L., Zhang, M., Hou, H., Song, Y., Wang, H., Zhong, B., Wang, L., 2017. Hierarchically mesostructured porous TiO2 hollow nanofibers for high performance glucose biosensing. Biosens. Bioelectron. 92, 654–660.
Hu, C.-M.J., Fang, R.H., Wang, K.-C., Luk, B.T., Thamphiwatana, S., Dehaini, D., Nguyen, P., Angsantikul, P., Wen, C.H., Kroll, A.V., Carpenter, C., Ramesh, M., Qu, V., Patel, S.H., Zhu, J., Shi, W., Hofman, F.M., Chen, T.C., Gao, W., Zhang, K., Chien, S., Zhang, L., 2015. Nanoparticle biointerfacing by platelet membrane cloaking. Nature 526, 118.
Huo, H., Guo, C., Li, G., Han, X., Xu, C., 2014. Reticular-vein-like Cu@Cu2O/reduced graphene oxide nanocomposites for a non-enzymatic glucose sensor. RSC Adv. 4 (39), 20459–20465.
Kim, I., Kwon, D., Lee, D., Lee, T.H., Lee, J.H., Lee, G., Yoon, D.S., 2018. A highly permselective electrochemical glucose sensor using red blood cell membrane. Biosens. Bioelectron. 102, 617–623.
Kim, S.N., Rusling, J.F., Papadimitrakopoulos, F., 2007. Carbon nanotubes for electronic and electrochemical detection of biomolecules. Adv. Mater. 19 (20), 3214–3228.
Kroll, A.V., Fang, R.H., Jiang, Y., Zhou, J., Wei, X., Yu, C.L., Gao, J., Luk, B.T., Dehaini, D., Gao, W., Zhang, L., 2017. Nanoparticulate delivery of cancer cell membrane elicits multiantigenic antitumor immunity. Adv. Mater. 29 (47), 1703969.
Lee, H., Hong, Y.J., Baik, S., Hyeon, T., Kim, D.-H., 2018. Enzyme-based glucose sensor: from invasive to wearable device. Adv. Healthc. Mater. 7 (8), 1701150.
Leonenko, Z.V., Carnini, A., Cramb, D.T., 2000. Supported planar bilayer formation by vesicle fusion: the interaction of phospholipid vesicles with surfaces and the effect of gramicidin on bilayer properties using atomic force microscopy. Biochim. Biophys. Acta Biomembr. 1509 (1), 131–147.
Lipani, L., Dupont, B.G.R., Doungmene, F., Marken, F., Tyrrell, R.M., Guy, R.H., Ilie, A., 2018. Non-invasive, transdermal, path-selective and specific glucose monitoring via a graphene-based platform. Nat. Nanotechnol. 13 (6), 504–511.
Liu, H., Xiang, Y., Lu, Y., Crooks, R.M., 2012. Aptamer-based origami paper analytical device for electrochemical detection of adenosine. Angew. Chem. Int. Ed. 51 (28), 6925–6928.
Mingeot-Leclercq, M.-P., Deleu, M., Brasseur, R., Dufrene, Y.F., 2008. Atomic force microscopy of supported lipid bilayers. Nat. Protoc. 3 (10), 1654–1659.
Raba, J., Mottola, H.A., 1995. Glucose oxidase as an analytical reagent. Crit. Rev. Anal. Chem. 25 (1), 1–42.
Rogers, M.L., Leong, C.L., Gowers, S.A., Samper, I.C., Jewell, S.L., Khan, A., McCarthy, L., Pahl, C., Tolias, C.M., Walsh, D.C., Strong, A.J., Boutelle, M.G., 2017. Simultaneous monitoring of potassium, glucose and lactate during spreading depolarization in the injured human brain – proof of principle of a novel real-time neurochemical analysis system, continuous online microdialysis. J. Cereb. Blood Flow Metab. 37 (5), 1883–1895.
Rosanwo, T.O., Kinney, M., Vo, L.T., Lundin, V., Daley, G.Q., 2017. Enucleation and beta-globin expression in induced red blood cells: a platform to model sickle cell anemia. Blood 130 (Suppl. 1), 538.
Shen, Z., Gao, W., Li, P., Wang, X., Zheng, Q., Wu, H., Ma, Y., Guan, W., Wu, S., Yu, Y., Ding, K., 2016. Highly sensitive nonenzymatic glucose sensor based on nickel nanoparticle–attapulgite-reduced graphene oxide-modified glassy carbon electrode. Talanta 159, 194–199.
Sode, K., Loew, N., Ohnishi, Y., Tsuruta, H., Mori, K., Kojima, K., Tsugawa, W., LaBelle, J.T., Klonoff, D.C., 2017. Novel fungal FAD glucose dehydrogenase derived from Aspergillus Niger for glucose enzyme sensor strips. Biosens. Bioelectron. 87, 305–311.
Soo, K.S., Kyeong, C.Y., Hee, H.M., Kyung, L.H., Jeong, K.Y., Ran, H.S., Hyun, L.J., Gong, L.S., Koo, P.Y., 2002. Clinical significance of glucose transporter 1 (GLUT1) expression in human breast carcinoma. Jpn. J. Canc. Res. 93 (10), 1123–1128.
Su, C.-K., Tseng, P.-J., Chiu, H.-T., del Vall, A., Huang, Y.-F., Sun, Y.-C., 2017. Sequential enzymatic derivatization coupled with online microdialysis sampling for simultaneous profiling of mouse tumor extracellular hydrogen peroxide, lactate, and glucose. Anal. Chim. Acta 956, 24–31.
Tamm, L.K., Tatulian, S.A., 1997. Infrared spectroscopy of proteins and peptides in lipid bilayers. Q. Rev. Biophys. 30 (4), 365–429.
Valdes, T.I., Moussy, F., 2000. In vitro and in vivo degradation of glucose oxidase enzyme used for an implantable glucose biosensor. Diabetes Technol. Ther. 2 (3), 367–376.
Vargas, E., Ruiz, M.A., Campuzano, S., Reviejo, A.J., Pingarrón, J.M., 2016. Non-invasive determination of glucose directly in raw fruits using a continuous flow system based on microdialysis sampling and amperometric detection at an integrated enzymatic biosensor. Anal. Chim. Acta 914, 53–61.
Venturelli, L., Nappini, S., Bulfoni, M., Gianfranceschi, G., Dal Zilio, S., Coceano, G., Del Ben, F., Turetta, M., Scoles, G., Vaccari, L., Cesselli, D., Cojoc, D., 2016. Glucose is a key driver for GLUT1-mediated nanoparticles internalization in breast cancer cells. Sci. Rep. 6, 21629.
Yang, J., Cho, M., Pang, C., Lee, Y., 2015. Highly sensitive non-enzymatic glucose sensor based on over-oxidized polypyrrole nanowires modified with Ni(OH)2 nanoflakes. Sensor. Actuator. B Chem. 211, 93–101.
Zhou, Y.-G., Rees, N.V., Compton, R.G., 2011. The electrochemical detection and characterization of silver nanoparticles in aqueous solution. Angew. Chem. Int. Ed. 50 (18), 4219–4221.